1   Carbon and Mercury Target Optimization with a 6.75 GeV Proton Driver

2   for the Intensity Frontier

3   X. Ding,[c*] H. G. Kirk,[a] J. S. Berg,[a] K.T. McDonald[b]

4   [a]Brookhaven National Laboratory, Upton, NY 11973, USA

5   [b]Joseph Henry Laboratories, Princeton University, Princeton, NJ 08544, USA

6   [c]Department of Physics, University of California, Los Angeles, CA 90095, USA

7

8   **Abstract**

9   A high power target is required to convert a powerful MW-class proton beam into an intense muon source

10   or neutrino source in support of physics at the intensity frontier. The first phase of a Muon Collider or

11   Neutrino Factory program may use a 6.75 GeV proton driver with beam power of only 1 MW. At this

12   lower power it is favorable to use a graphite target with beam and target tilted slightly to the axis of the 20

13   T pion-capture solenoid around the target. Using the MARS15 (2014) code with ROOT-based geometry

14   setting, we optimize the geometric parameters of the beam and target to maximize particle

15   production at low energies by incoming proton beam with kinetic energy of 6.75 GeV and rms

16   geometric emittances of 0, 5, 20 and 50 mm-mrad impinging on this carbon target. The optimization

17   shows that the particle production decreases slowly with increasing emittance. We study beam-dump

18   configurations to suppress the rate of undesirable high-energy secondary particles in the beam. For a

19   possible upgrade to a proton beam of multi-MW power, we consider a free-flowing mercury jet. We report

20   on optimization of particle production by a mercury target inside the scenario of 15 T pion-capture solenoid

[*] Corresponding author. Tel.: +16313444635
   Email addresses: xding@bnl.gov.

around the target. We compare the quantity of generated muons using a mercury jet target to that from a carbon target.

1. Introduction

Neutrino-physics and muon-physics at the intensity frontier require the greatest possible beam intensities of neutrinos and muons. The ultimate option for the final stage of a possible future Muon Collider (MC) or Neutrino Factory (NF) [1] in the Muon Accelerator Program [2] is to use a 4 MW proton beam interacting with a free-flowing mercury jet to create copious amounts of pions that are captured in a high-field solenoid magnet system (~ 20 T). The pions are then transported into a tapered solenoid decay channel in which decay muons will be captured, cooled and stored in a storage ring, either to provide for $\mu^+\mu^-$ collisions or to produce intense neutrino beams. The target scenario for the present study in the first phase of the Muon Accelerator program recommended by the Muon Accelerator Staging Study (MASS) [2] is to use a 6.75 GeV proton driver with beam power of 1 MW interacting with a graphite target in the so-called 20to2T5m target system configuration, as shown in Fig. 1.

Fig. 2 shows that the axial magnetic field for configuration 20to2T5m tapers adiabatically over 5 m from 20 T around the target to 2 T in the rest of Front End [3, 4]. The inner radius of superconducting coils (SC) in the region surrounding the graphite target is 120 cm (up from 60 cm in [5]) to permit sufficient internal tungsten shielding for a 10-year operational lifetime of the SC coils against radiation damage [6]. The first 50 m of the magnetic channel of the Front End is sketched in Fig. 3.

15 T superconducting coil outsert,
Stored energy ~ 3 GJ, ~ 100 tons

Last
Final-Focus
quad

Proton
bcam
tube

Upstream
proton beam
window

5 T copper-coil insert,
Water-cooled, MgO insulated

Target/dump vessel

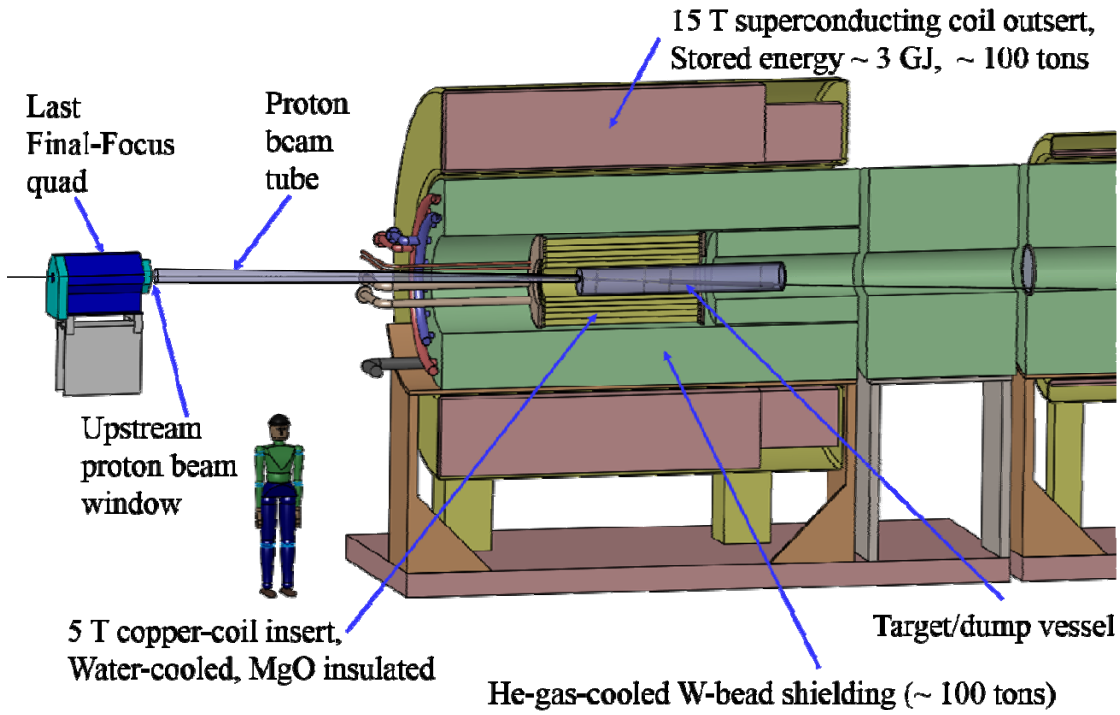He-gas-cooled W-bead shielding (~ 100 tons)

1
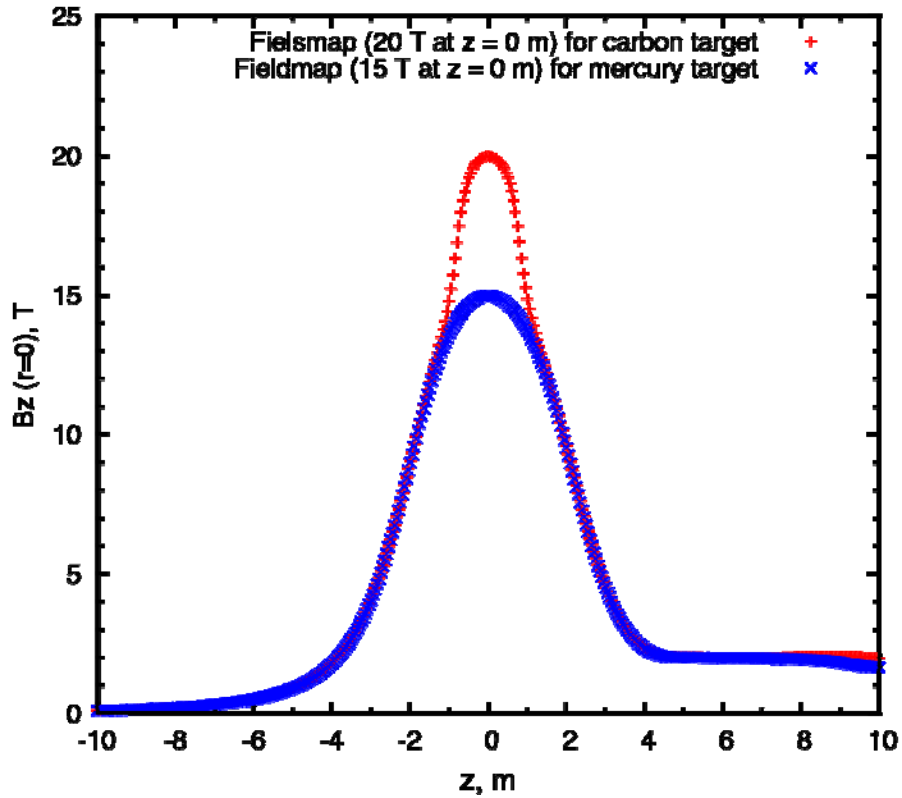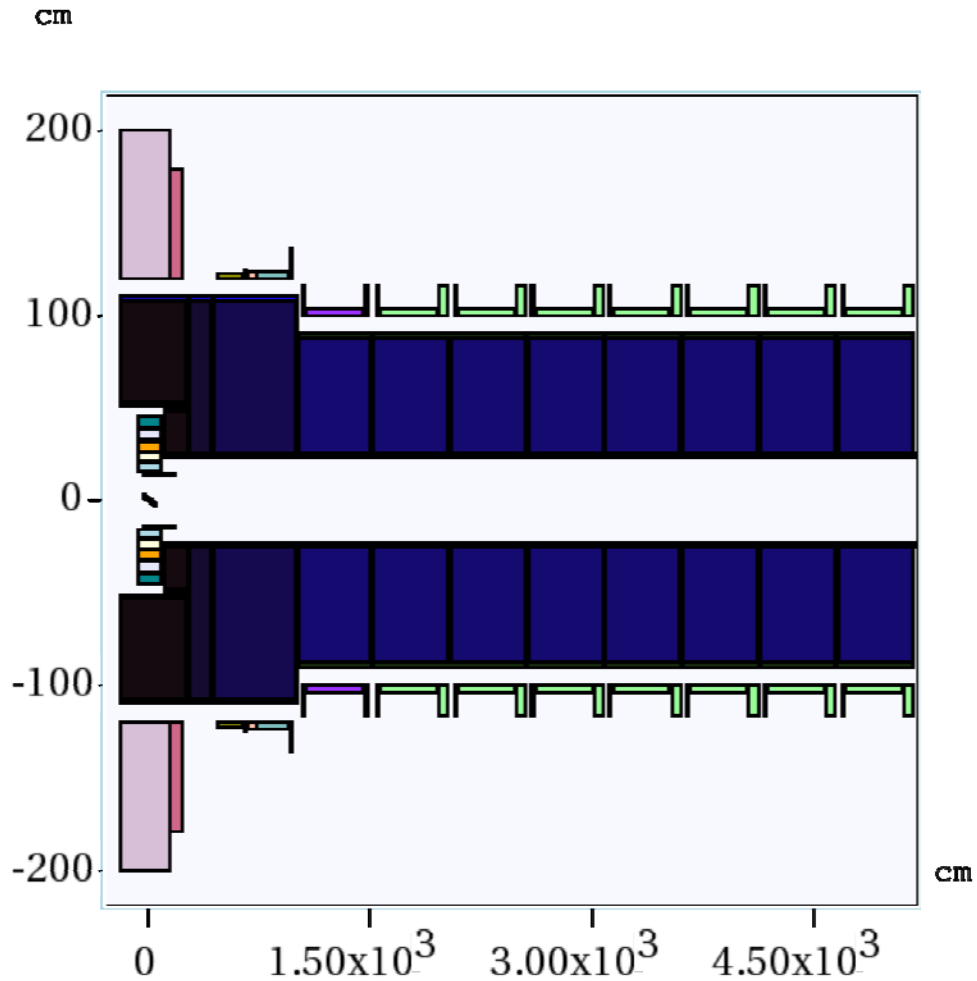2   Figure 1: Layout of the 20to2T5m Target System configuration.

3
4   Figure 2: Axial magnetic field of the 20to2T5m (red dots for carbon) and 15to2T5m (blue dots for

5   mercury) Front-End channels. The center of the target is at z = 0.

cm

200 —

100 —

0 —

-100 —

-200 —

cm

0   1.50x10³   3.00x10³   4.50x10³

y

↑
↳ z

y:z = 1:1.250e+01

Figure 3: Schematic of the 20to2T5m Carbon Target System configuration, for -2 < z < 50 m.

The graphite-target, and graphite-beam-dump, rods are inside a double-walled stainless-steel containment vessel, with downstream Be windows, shown in Fig. 4. These rods are radiation cooled, and the containment vessel is cooled by He-gas flow between its double walls. The outer cylinder extends over -46 < z < 170 cm, with outer radius r = 15 cm. The inner cylinder extends over -45 < z < 169 cm, with inner radius r = 14 cm. The downstream faces of the vessels are Be windows, ≈ 1 mm thick.
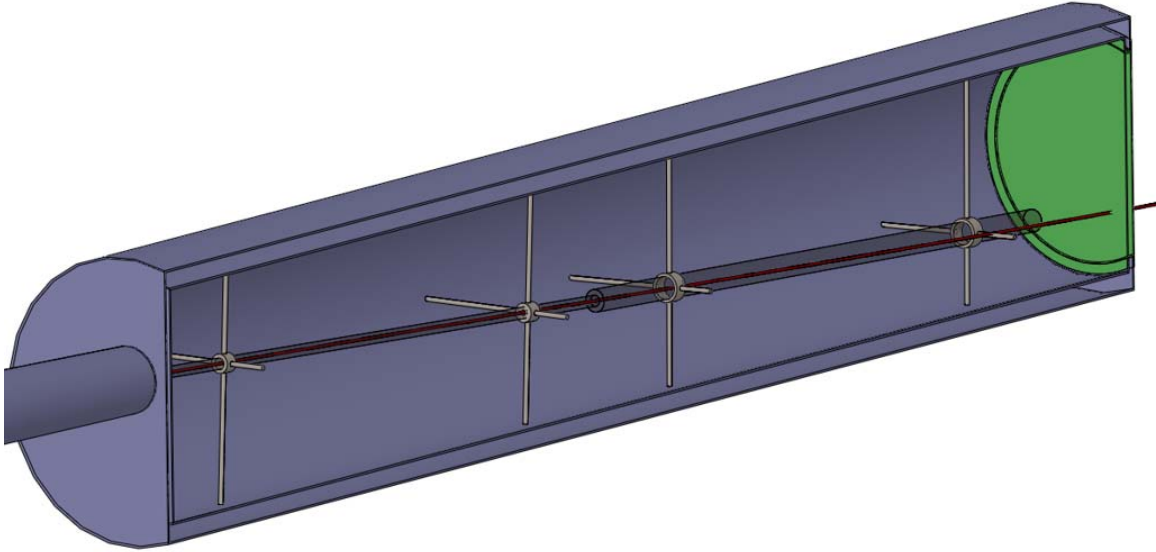
1

2   Figure 4: The carbon-target and dump rod inside the double-walled stainless-steel containment

3   vessel, with downstream Be window. The proton beam and carbon target cross at z = 0 cm. The

4   proton beam is launched at z = −100 cm in the simulation.

5

6   The Front End for 5 < z < 50 m consists of nine 5-m-long superconducting magnet modules,

7   each with internal tungsten shielding around the 23-cm-radius beam pipe. The latter has thin Be

8   windows, ≈ 0.05 mm thick, at each end of a magnet module, and is filled with He gas at 1

9   atmosphere.

10   The particle production at the end of decay channel of a front end depends on the length and

11 radius of the target, the radius of the proton beam, the orientation of the proton beam relative to

12 the magnetic field, and the angle of the beam and target relative to each other (both of which lie

13 in a vertical plane) [7]. Our previous study also shows that more particle production (about 20%)

14 can be generated if the end field in the front end is increased from 2T to 4T [8]. We will study not

15 only the 20to2T5m but also the 20to4T5m solenoid capture configuration and optimize their

16 particle production for further front end feasibility study. The first 50 m of the magnetic channel

17 of the Front End in the 20to4T5m configuration is sketched in Fig. 5.

18

cm

cm

y

z
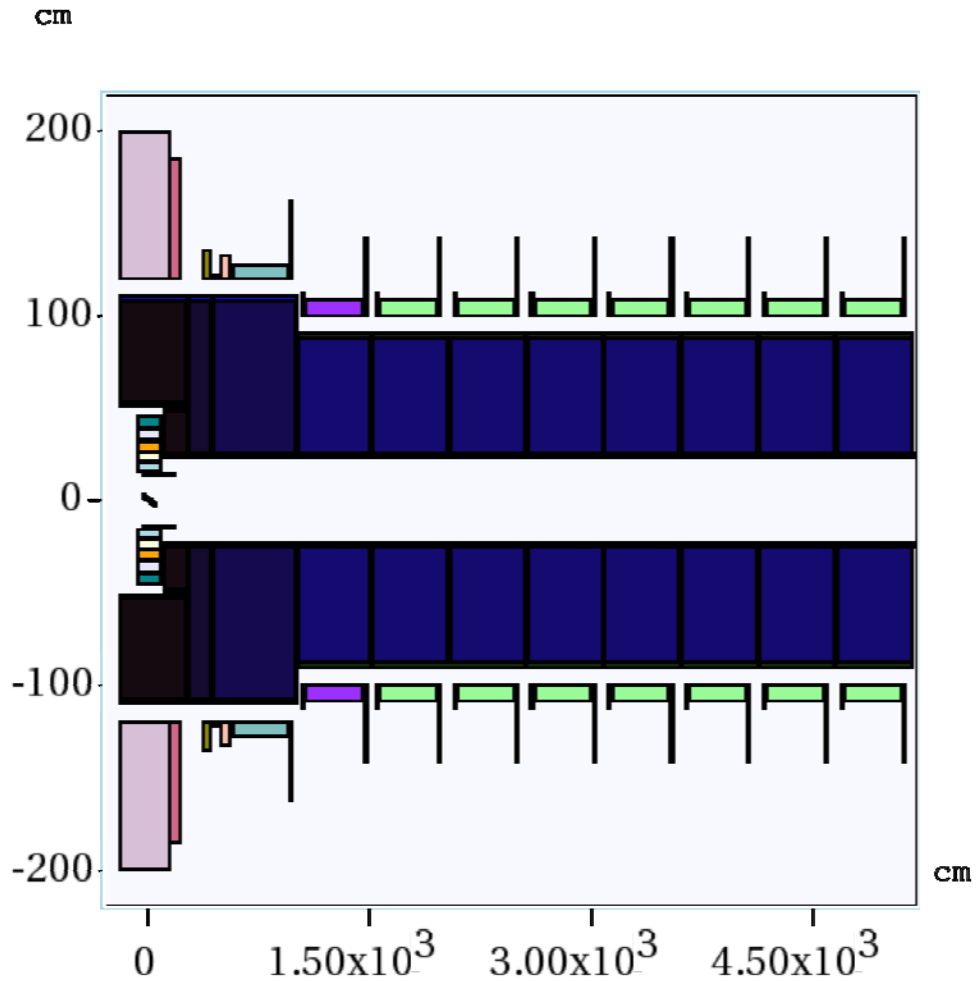
y:z = 1:1.250e+01

Figure 5: Schematic of the 20to4T5m Carbon Target System configuration, for -2 < z < 50 m.

For a possible upgrade to a proton beam of multi-MW power, at which the operational life of a graphite target might be undesirably short, we considered a free-flowing mercury jet in the so-called 15to2T5m or 15to4T5m configuration, which would evolve from the 20Tto2T5m or 20to4T5m configuration by extracting the C target/dump vessel and the 5 T copper coil insert (which is not physically compatible with the mercury-target infrastructure), and inserting a mercury target vessel in their place (z < 4.5 m, r < 23 cm). The validity of the liquid target

1   concept has been demonstrated in the MERIT high intensity liquid mercury target experiment [9].

2   Fig. 6 shows that the axial magnetic field for all four configurations of 20to2T5m, 20to4T5m,

3   15to2T5m and 15to4T5m tapers adiabatically over 5 m from 20 T or 15 T around the target to 2 T

4   or 4 T in the rest of Front End.
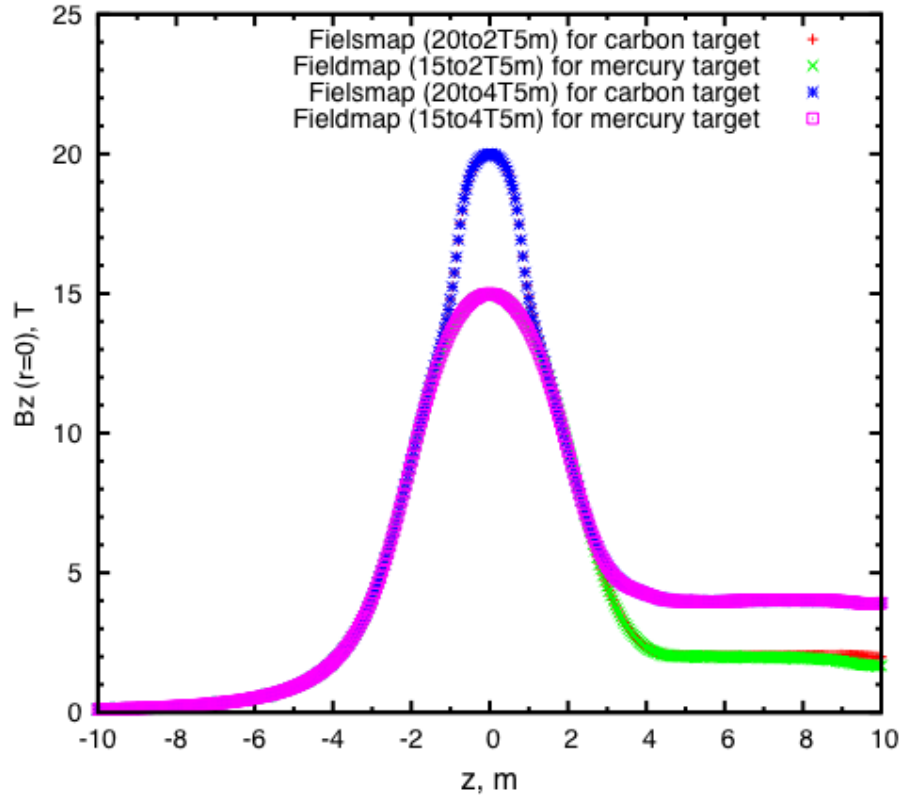
5

6   Figure 6: Axial magnetic field of the 20to2T5m, 20to4T5m, 15to2T5m and 15to4T5m Front-End

7   channels. The center of the target is at z = 0.

8

9   In the present paper, we will report our efforts on both carbon and mercury target

10   optimization with a 6.75 GeV proton driver using the MARS15 (2014) code [10] with ROOT-

11   based geometry setting. Section 2 describes an optimization study of these geometric beam and

12   target parameters for a carbon target with 20to2T5m target system configuration. In Section 3, we

13   optimize the carbon target with 20to4T5m configuration. In Section 4, we compare the yield

14   between tilted carbon target and zero-deg carbon target in configuration 20to2T5m and 20to4T5m

with peak field of 20 T. In section 5, we consider a free-flowing mercury jet as a possible upgrade to a proton beam of multi-MW power, at which the operational life of a graphite target might be undesirably short. We report on optimization of particle production by a mercury target in the 15to2T5m and 15to4T5m configuration. In Section 6, we study beam-dump configurations to suppress the rate of undesirable high-energy secondary particles in the beam, finally, we conclude with a summary in Section 7.

2. Carbon target optimization in configuration 20to2T5m with peak field of 20 T

The MARS15(2014) code [4] with its default setting for event generation (IQGSM = 1) and configuration 20to2T5m setting with a ROOT-based geometry description were used for target optimization. Fig. 7 shows a schematic of the carbon target geometry. The center of the target is at (0, 0, 0) cm. We consider a focused 6.75GeV proton beam by assuming the focal point is at $z = 0$ where the beam has Twiss parameters $\alpha^* = 0$, β^*, rms radius σ^* and (geometric) transverse emittance $\varepsilon = \sigma^{*2}/\beta^*$. The proton beam was launched at $z = -100$ cm so as to have the above specified rms transverse emittance, beam angle and waist at the center of the target ($z = 0$), after propagating in the magnetic field. For this, an antiproton beam was generated at $z = 0$ with the specified parameters, propagated back to $z = -100$ cm without a target, and then the charge and momentum was reversed, and the target restored, for subsequent propagation in the positive z direction.
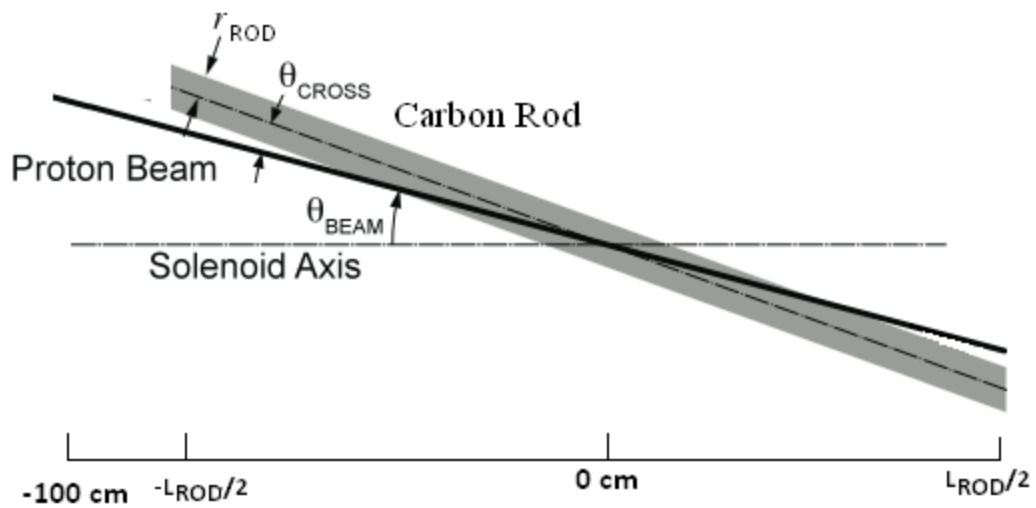
Figure 7. The carbon-target geometry. The focal proton beam waist is at the center of the target at z = 0.
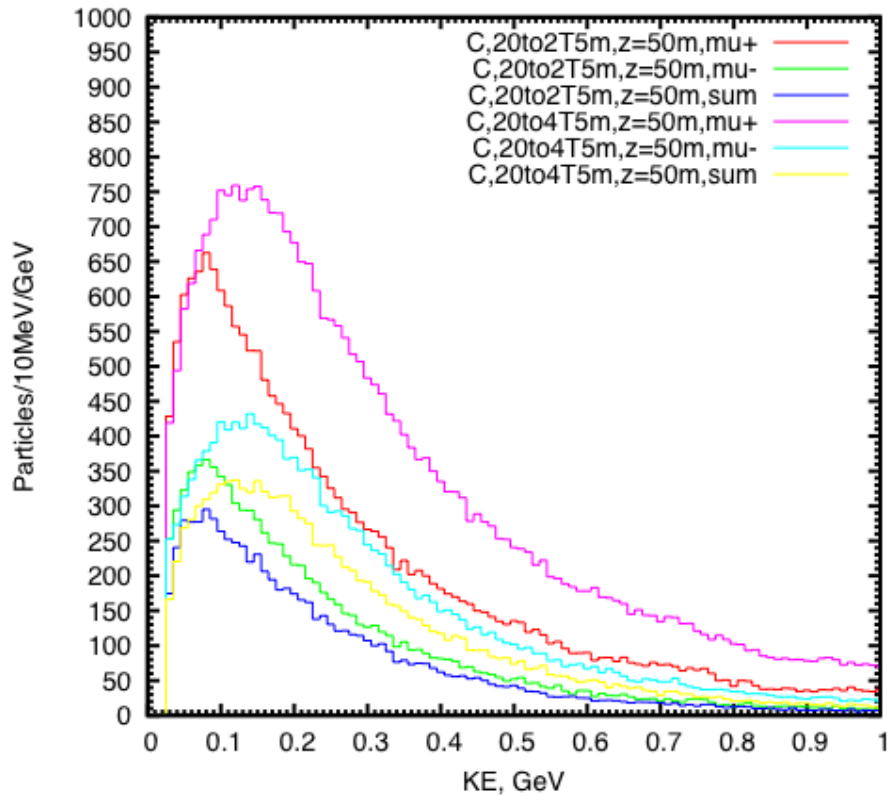
Figure 8. Muon energy spectra at z = 50 m. Data points represent muons generated from 4×10^5 incoming 6.75 GeV protons in both 20to2T5m and 20to4T5m configuration.

9

1   The particle production of interest to a Muon Collider/Neutrino Factory is defined to be the

2   collection of charged muoned and charged pions with kinetic energies between 40 and 180 MeV

3   or between 40 and 300 MeV at the end of a 50 m decay channel (see Fig. 8). The optimization

4   used here is based on maximizing the yield of these particles at the plane $z = 50$ m, which is near

5   the beginning of the Buncher of the Front-End [3].

6   The graphite density was assumed to be 1.8 g/cm^3. The initial target radius was chosen as

7   0.75 cm and the target angle as 50 mrad to the solenoid axis of the SC coils [11]. The target and

8   beam were tilted by the same angle with respect to the solenoid axis, while the beam radius (rms

9   spot size) was fixed to be one-fourth of the target radius. The trajectory of the proton beam in the

10   magnetic field is helical, and this trajectory is collinear with target axis on at the center of the

11   target ($z = 0$). For our optimization method, several runs were performed during each

12   optimization cycle. In run 1 we varied the target length while keeping initial target radius, target

13   angle fixed; in run 2 we varied the target radius using the new target length while keeping the

14   target angle fixed; and in run 3 we varied the target angle with the new target radius. We repeated

15   the above until convergence was achieved.

16   Fig. 9 depicts the particle production as a function of target length, which shows that the

17   yield increased with the target length, saturating for lengths larger than about 100 cm.
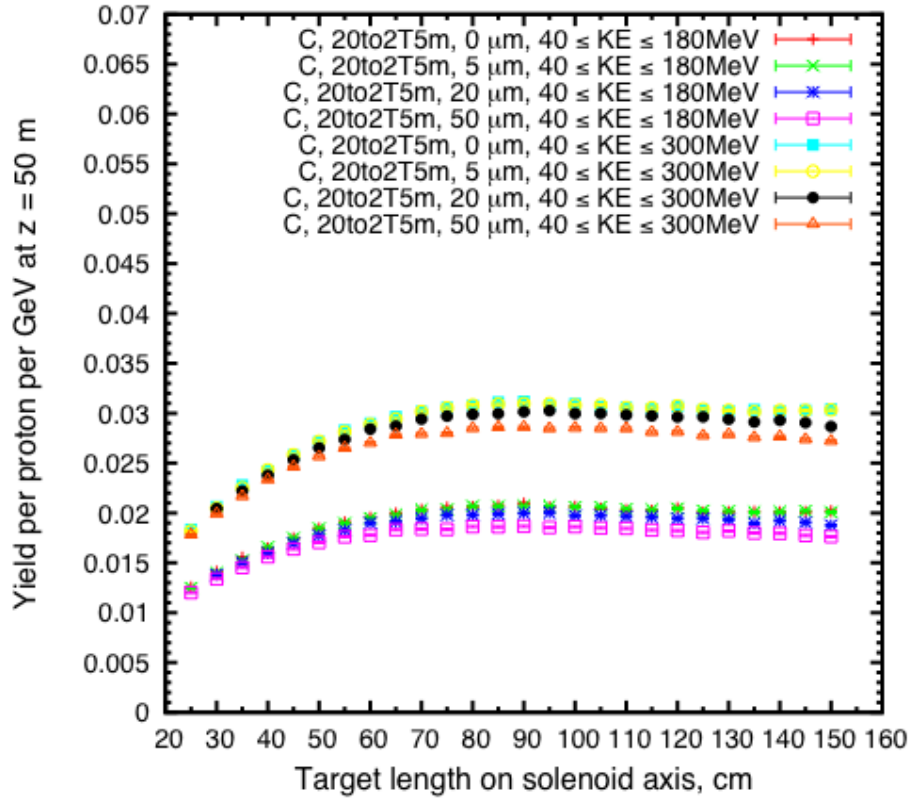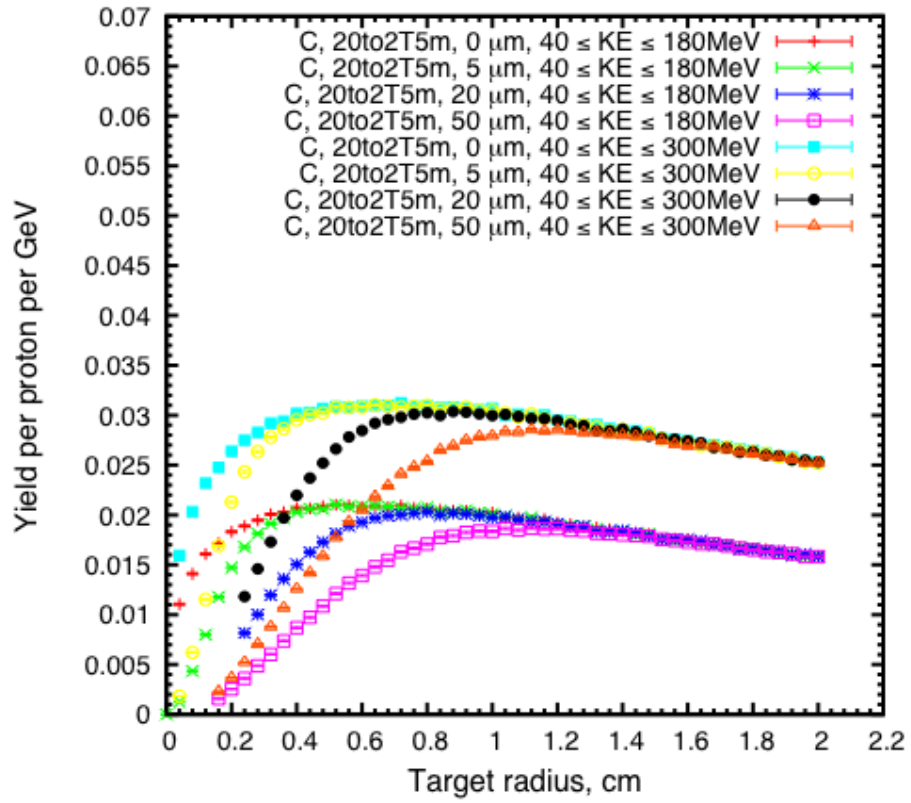
Figure 9. Muon yield at z = 50 m as a function of target length for different rms geometric emittance (target tilt angle is 65 mrad; target radii are 0.8 cm for both 0 and 5 μm emittance, 1 cm for 20 μm emittance and 1.2 cm for 50 μm emittance).

Fig. 10 shows the variation of particle production with target radius. The production is maximized when the target has a radius of 1 cm for a fixed rms geometric emittance of 20 mm-mrad. The optimization shows that the particle production decreases only slowly with increasing emittance. The yield for 50 μm emittance and target radius of 1.2 cm is only 10% less than that for the nominal case of 5 μm emittance and 0.8 cm target radius.
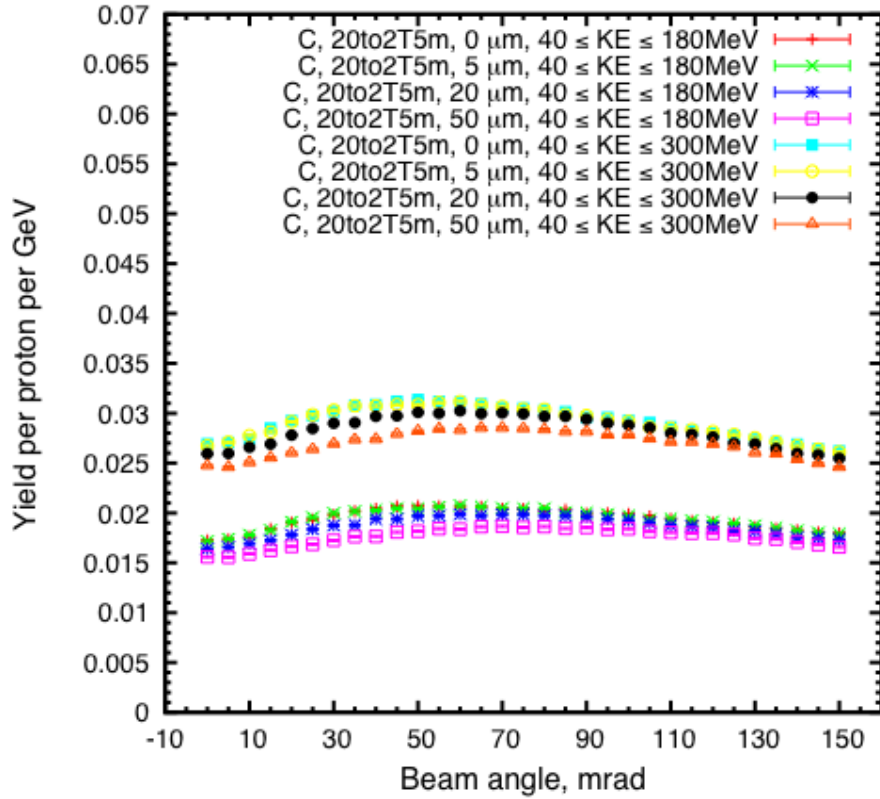
Fig. 11 shows the particle production as a function of beam angle, with a peak around 65 mrad.

1

Figure 10. Muon yield at z = 50 m as a function of target radius for different rms geometric

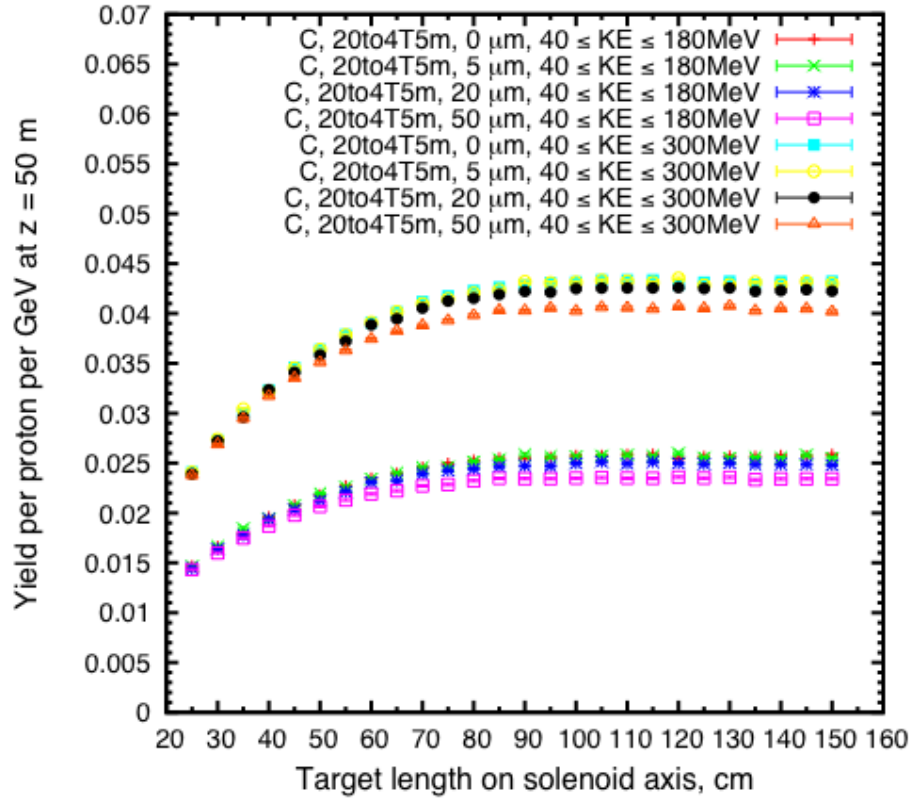emittance (target length is 100 cm and tilt angle is 65 mrad).

Figure 11. Muon yield at z = 50 m as a function of beam angle for different rms geometric

emittance (target length is 100 cm; target radii are 0.8 cm for both 0 and 5 μm emittance, 1 cm for
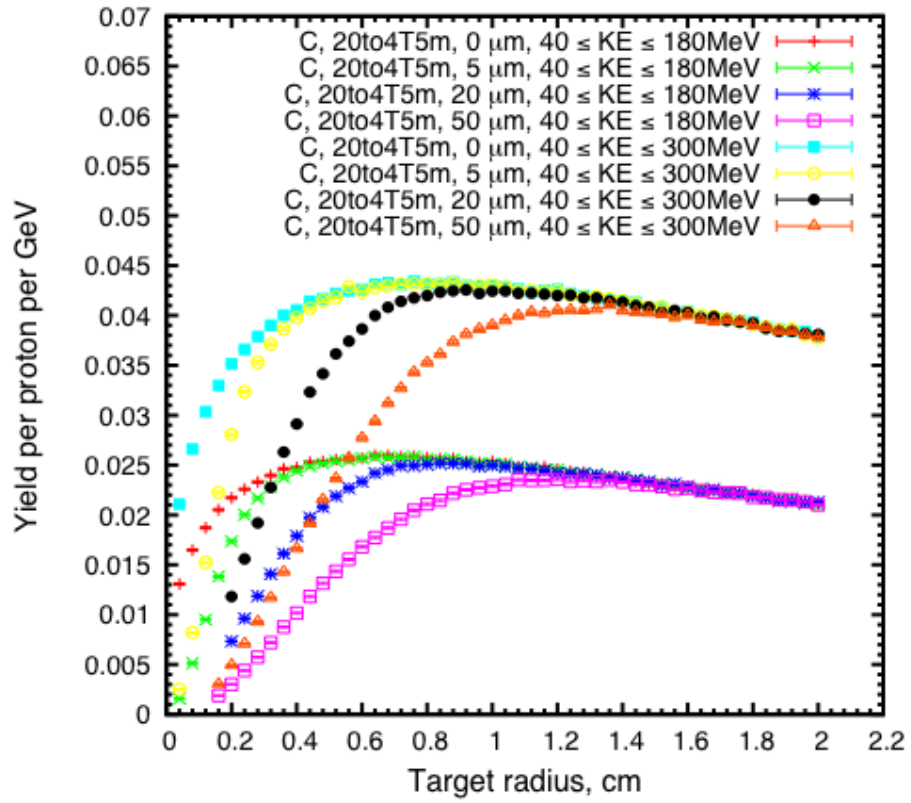
20 μm emittance and 1.2 cm for 50 μm emittance).

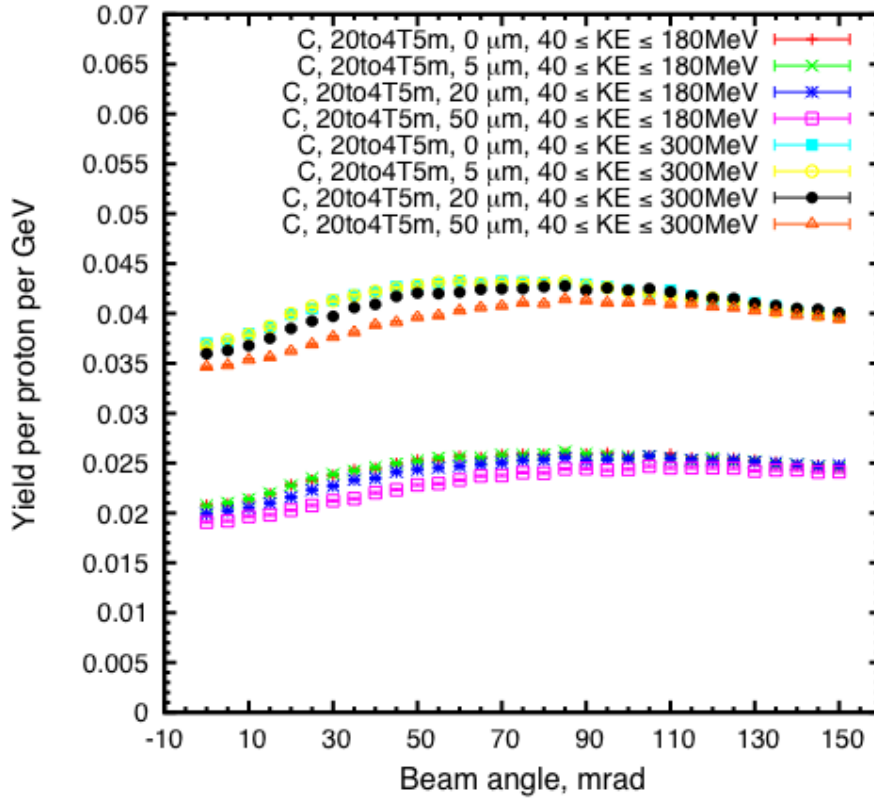## 3. Carbon target optimization in configuration 20to4T5m with peak field of 20 T

We also optimized the carbon target in configuration 20to4T5m. The particle productions as

a function of target length, the target radius and target tilt angle are shown in Fig.12, Fig.13 and

Fig.14, respectively.

Figure 12. Muon yield at z = 50 m as a function of target length for different rms geometric

emittance (target tilt angle is 65 mrad; target radii are 0.8 cm for both 0 and 5 μm emittance, 1 cm

for 20 μm emittance and 1.2 cm for 50 μm emittance).

1

2   Figure 13. Muon yield at z = 50 m as a function of target radius for different rms geometric

3   emittance (target length is 100 cm and tilt angle is 65 mrad).

1

Figure 14. Muon yield at z = 50 m as a function of beam angle for different rms geometric

emittance (target length is 100 cm; target radii are 0.8 cm for both 0 and 5 μm emittance, 1 cm for

20 μm emittance and 1.2 cm for 50 μm emittance).

4. Tilted carbon target vs. zero-deg carbon target in configuration

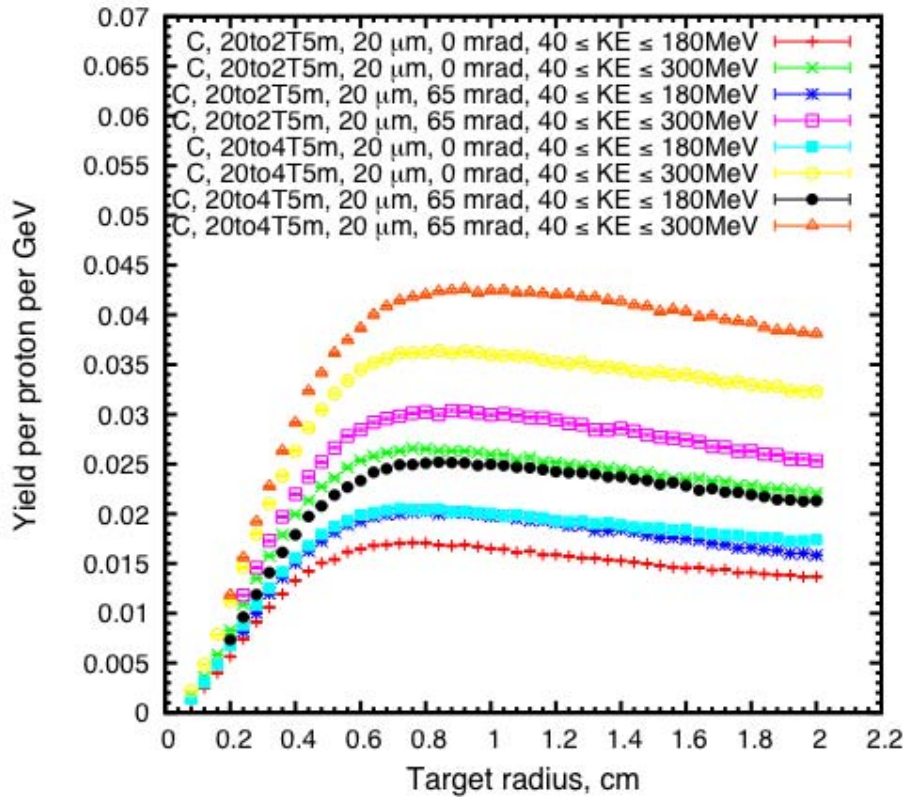## 20to2T5m and 20to4T5m with peak field of 20 T

We also optimized the carbon target without tilt to the axis of SC coils in configuration 20to

2T5m and 20to4T5m. Fig. 15 shows the particle production as a function of target radius at rms

geometric emittance of 20 μm.

Figure 15. Comparison of tilted carbon target vs. zero-deg carbon target of muon yield at $z = 50$ m as a function of target radius for rms geometric emittance of 20 μm (target length is 100 cm).

5. Mercury target optimization in configuration 15to2T5m and 15to4T5m with peak field of 15 T

We optimized the target parameters for a 6.75 GeV and rms geometric emittance of 20 μm proton beam impinging on a mercury jet with assumed length of 100 cm in the configurations of 15to2T5m and 15to4T5m. The target and beam were tilted at different angles with respect to the magnetic axis, while the rms beam radius at $z = 0$ cm was fixed to be 30% of the target radius.

Fig. 16 shows the variation of muon yield with target radius for mercury target. The production was maximized when the target had a radius around 0.5 cm.
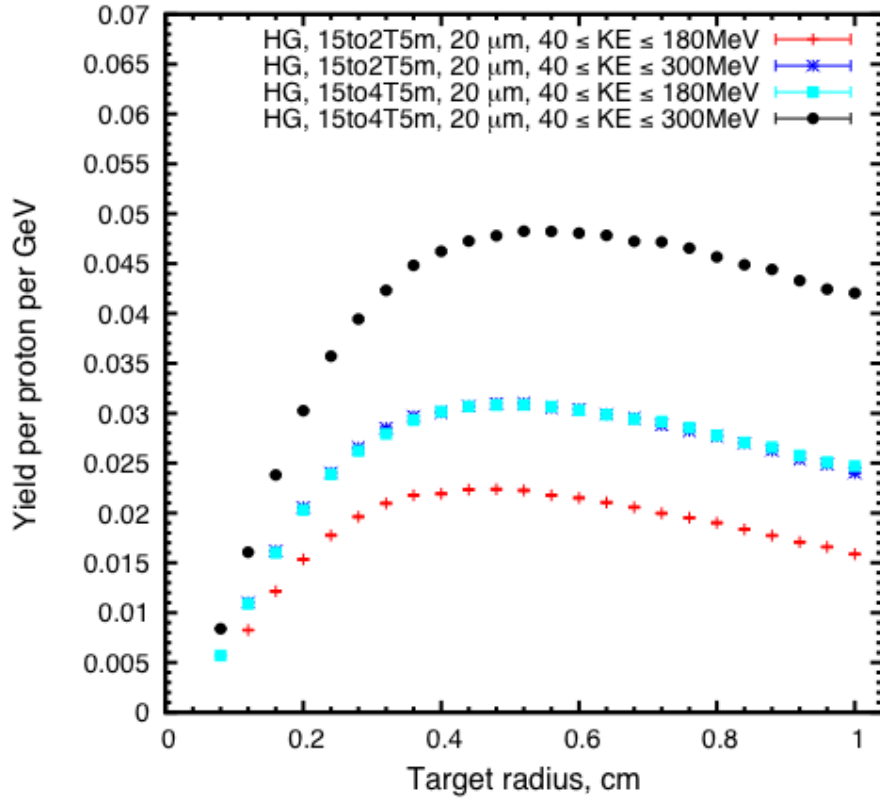
Figure 16. Muon yield at z = 50 m as a function of target radius (beam tilt angle is 65 mrad and beam/jet crossing angle is 24 mard).

Fig. 17 shows that the yield increased with the proton- beam angle, saturating for angles larger than about 65 mrad. This is favorable, in that it would be desirable to use the same incident proton beam in a mercury-target option as in the initial carbon-target configuration.

1
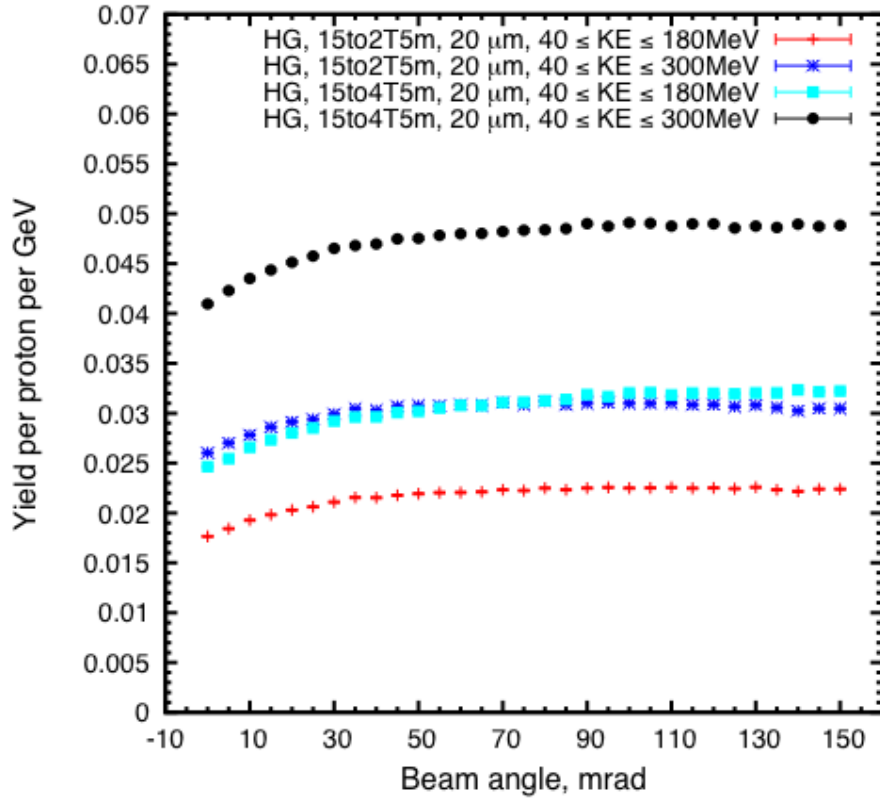
Figure 17. Muon yield at z = 50 m as a function of beam angle (target radius is 0.5 cm and jet/beam

crossing angle is 24 mrad).

Fig. 18 shows the yield as a function of beam/target crossing angle, which peaked around 24

mrad. The mercury-jet angle would be larger than the proton-beam angle, and hence about 89

mrad to the magnetic axis. This larger angle would facilitate collection of the mercury jet in a

pool that also serves as the proton-beam dump for the mercury-target configuration.
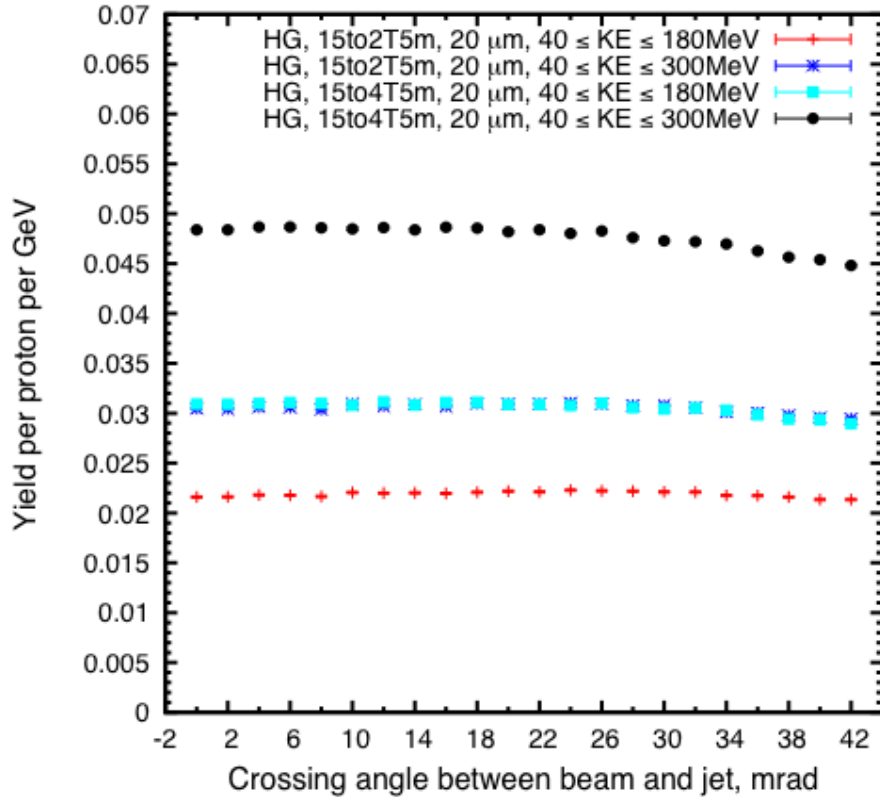
Figure 18. Muon yield at $z = 50$ m as a function of beam/jet crossing angle (target radius is 0.5 cm and beam tilt angle is 65 mrad).

6. Design of graphite beam dump

We also designed a graphite proton-beam dump to intercept the (diverging) unscattered protons from incoming beam with rms geometric emittance of 20 μm. The beam dump consisted of two segments. Each was a rod with length of 55 cm. The first rod extended over $50 < z < 105$ cm with a radius of 3 cm and its centers of end faces at x = (0, -3.2, 50) and (-2.5, -6.2, 105) cm. The second rod extended over $105 < z < 160$ cm with a radius of 4 cm and its centers of end faces at (-2.5, -6.2, 105) and (-5.0, -8.6, 160) cm. The beam dump would intercept about ~65% of the (diverging) unscattered proton beam with kinetic energy above 6 GeV while causing only 12% decrease in the yield. Fig. 19 shows the schematic of incoming unscattered proton beam (6.75 GeV without interaction with target) and scattered proton beam (KE above 6 GeV with interaction with target) at the center of target, end of target, end of first section and second section

1 of beam dump (10000 incoming protons with rms geometric emittance of 20 μm and 20to4T5m

2 configuration).

3
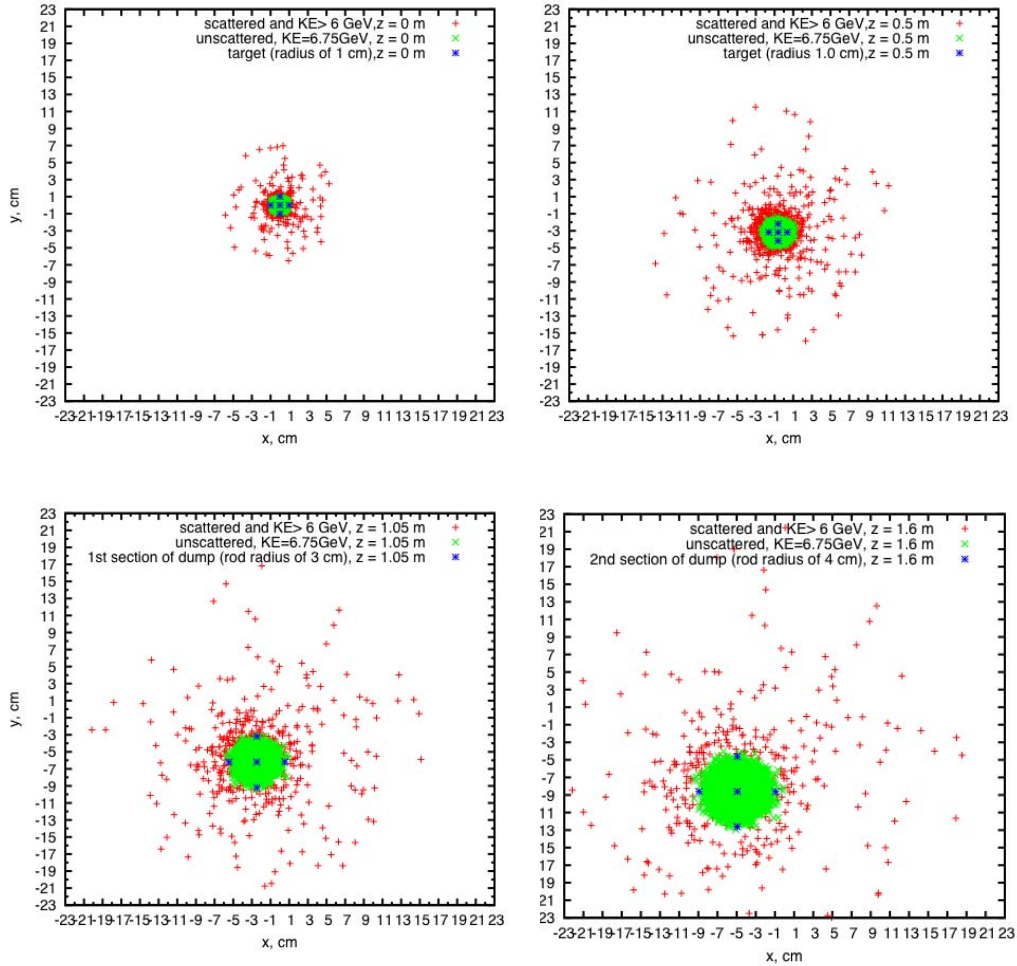
18 Figure 19: Schematic of unscattered and scattered beam at the center of target, end of the target, end

19 of first and section of beam dump in the 20to4T5m Carbon Target System configuration (10000 proton

20 events with rms geometric emittance of 20 μm used).

21

7. Conclusions

23   With a 6.75-GeV incident proton beam, we optimized both a carbon target in the 20to2T5m

24 and 20to4T5m (20-T peak field) and a mercury target in the 15to2T5m and 15to4T5m

25 configuration (15-T peak field). For rms transverse, geometric beam emittance at 20 mm-mrad,

the optimized parameters for a carbon target are: target length 100 cm, target radius 1.0 cm, beam radius 0.25 cm, beam angle 65 mrad and target angle 65 mrad; while for a mercury-jet target they are: target radius 0.5 cm, beam radius 0.15 cm, beam angle 65 mrad and beam/Hg jet crossing angle 24 mrad. The mercury target is also predicted to give more yield than the carbon target.

In addition, the study showed that the yield would decrease only very slowly with increasing transverse emittance of the proton beam, such that good performance is compatible with the use of larger emittance proton beams.

Furthermore, the study for the graphite target included consideration of a graphite proton-beam dump, modelled in ROOT-based geometry.

References

[1] M. Alsharo'a *et al.*, Phys. Rev. ST Accel. Beams **6**, 081001 (2003).

[2] M.A. Palmer *et al.*, Proc. IPAC13, TUPFI057, p. 1475.

[3] J.S. Berg *et al.*, Phys. Rev. ST Accel. Beams **9**, 011001 (2006).

[4] H.K. Sayed *et al.*, Proc. IPAC13, TUPFI075, p. 1520.

[5] S. Ozaki, R.B. Palmer, M.S. Zisman, and J.C. Gallardo, BNL-52623 (2001).

[6] N. Souchlas *et al.*, Proc. IPAC11, TUPS054, p. 1653.

[7] X. Ding *et al.*, Phys. Rev. ST Accel. Beams **14**, 111002 (2011).

[8] H.K. Sayed *et al.*, Proc. IPAC14, MOPRI007, p. 589.

[9] K.T. McDonald *et al.*, Proc. PAC09, TU4GRI03, p. 795.

1   [10] N.V. Mokhov, Fermilab-FN-628, 1995; N.V. Mokhov and S. I. Striganov, in Proceedings of

2   the Hadronic Shower Simulation Workshop, Fermilab (2006) [AIP Conf. Proc. 896, 50 (2007)],

3   http://www-ap.fnal.gov/MARS/.The MARS Code System: http://www-ap.fnal.gov/MARS/

4   [11] N.V. Mokhov, Nucl. Instr. And Meth. A 472, 546 (2001).